Biogeosciences Discussions, 2, 103–136, 2005
www.biogeosciences.net/bgd/2/103/
SRef-ID: 1810-6285/bgd/2005-2-103
European Geosciences Union

Biogeosciences Discussions is the access reviewed discussion forum of *Biogeosciences*

Diatoms and their influence on the biologically mediated uptake of atmospheric CO_2 in the Arabian Sea upwelling system

T. Rixen[1], **C. Goyet**[2], **and V. Ittekkot**[1]

[1]Center for Tropical Marine Ecology, Fahrenheitstr. 6, 28359 Bremen, Germany
[2]Université de Perpignan, Bât. B., BDSI, 52 avenue Paul ALDUY, 66860 Perpignan, France

Received: 17 December 2004 – Accepted: 13 January 2005 – Published: 25 January 2005

Correspondence to: T. Rixen (trixen@zmt-bremen.de)

Abstract

Model experiments have shown that diatoms can lower the atmospheric CO_2-concentration when they grow at the expense of coccolithophorids, since this reduces the precipitation of calcium carbonate, which acts as an oceanic CO_2 source. In the Arabian Sea we conducted long-term sediment trap experiments (water depth >1000 m) in order to study processes controlling shifts from diatom to non-diatom dominated systems. One of our major problems was to link sediment trap records to surface ocean processes. Satellite-derived observations on upper ocean parameters were helpful to reduce this problem in the past and gain a new quality by combining it with results obtained during the Joint Global Ocean Flux Study in the Arabian Sea. The new results imply that a deficiency of silicon (Si) in the euphotic zone terminates diatom blooms. Enhanced eolian iron inputs raise the availability of silicon in the surface water by decreasing the Si/N uptake ratios of diatoms. An enhanced abundance of diatoms within the plankton community seems to increase the biologically mediated uptake of atmospheric CO_2 by suppressing blooms of calcium carbonate producing organisms and by elevating the carbon to nutrient uptake (Redfield) ratio. These results agree in principle with assumptions made in models but indicate also that enhanced iron concentrations hinder the development of diatom blooms. The latter could be responsible for the amplitude of derived changes in the Redfield ratio and in the ratio between organic carbon and calcium carbonate carbon production which fall below assumptions made in some model experiments.

1. Introduction

Marine organisms influence ocean/atmospheric CO_2 exchange by photosynthesising organic matter and by precipitating carbonate shells. The subsequent export of organic carbon and calcium carbonate into the deep sea and the resulting net effect on the atmospheric CO_2 concentration is defined as the biological pump (Volk and Hoffert,

1985). The biological pump is driven by nutrients such as phosphate and inorganic nitrogen (N = nitrate + nitrite + ammonia), which are, in addition to carbon, required to build up organic matter (Heinze et al., 1991; Maier-Reimer et al., 1996; Tyrrell, 1999; Hedges et al., 2002). The efficiency of the biological pump can be enhanced by raising the uptake ratio of carbon to nutrients (C/N/P Redfield ratio) during the production of organic matter and by a reduction of the calcium carbonate precipitation, because the latter process increases the CO_2 concentration in sea water (Redfield et al., 1963; Berger and Keir, 1984; Heinze et al., 1991). Depending on the species and on environmental conditions the C/P ratio of marine organisms varies between 40 and >200 (Goldman et al., 1979; Burkhardt et al., 1999; Greider and La Roche, 2002; Klausmeier et al., 2004). Nevertheless, despite such variations, a global analysis suggests a mean Redfield ratio of 117±14/16±1 (Anderson and Sarmiento, 1994), which is close to the constant Redfield ratio derived by a 'General Circulation Model' (GCM; 122/16/1; Maier-Reimer, 1996), and to those found by a basin-wide analysis in the Arabian Sea (125:14:1; Millero et al., 1998).

Carbonate production is often parameterised by applying a fixed ratio between the organic carbon production and the precipitation of calcium carbonate carbon (rain ratio). Data-based estimates of rain ratios are scarce and deviate between 3.3 and 12.5 (Sarmiento et al., 2002; and references therein). A new estimate even suggests a mean global rain ratio of 16 (Sarmiento et al., 2002). All these estimates fall within the range of global mean rain ratios (2.3 to 26.6), which can be obtained by dividing the global mean organic carbon export derived from satellite data (2 to 16 $10^{15}\,g\,C\,yr^{-1}$; Falkowski et al., 2000; Rixen et al., 2002) by estimates of the global mean carbonate carbon export (Table 1).

Possible effects of changing Redfield and rain ratios on the atmospheric CO_2 concentration were quantified using GCMs. It was estimated that an increase of the C/P ratio by 30% (122:1 to 158.6:1) could lower the atmospheric CO_2 concentration by ~72 ppm (Heinze et al., 1991). A doubling of the global mean rain ratio from 4 to 8 could reduce the atmospheric CO_2 concentration by 28.5 ppm (Heinze et al., 1991) , and raising

the rain ratio from 5 to 16.6 could, however, reduce the atmospheric CO_2 concentration by 70 ppm (Archer et al., 2000). Such changes explaining a major proportion of the glacial/interglacial variation of the atmospheric CO_2 concentration were achieved by assuming that diatoms outcompete the carbonate-producing coccolithophorids and drive the export production. Since diatom growth is believed to be limited by the availability of silicon at lower latitudes (Dugdale and Wilkerson, 1998; Rixen et al., 2000), changes of the global silicon cycle and re-organisation of the marine silicon cycle were proposed as being possible mechanisms to fertilise lower latitudes with silicon during glacial times (Froelich et al., 1992; Harrison, 2000; Conley, 2002; Ridgwell et al., 2002). The re-organisation of the marine silicon cycle is suggested to be triggered by an enhanced eolian iron input lowering the Si/N uptake ratio of diatoms in the Southern Ocean and, subsequently, enhancing the silicon export from higher to lower latitudes (Matsumoto and Sarmiento, 2002).

In addition to coccolithophorids competing with diatoms, there are also carbonate-producing heterotrophs like foraminifera and pteropods which feed on diatoms. In the Arabian Sea sediment trap experiments showed that the peak flux of foraminifera into the deep sea coincides with that of diatoms in the highly productive upwelling system (Haake et al., 1993a, b). Of course, this could be an independent co-occurrence due to the enhanced production of organic matter, but it could also result from ecological advantages of foraminifera over other herbivores during diatom blooms. Diatoms can, for instance, reduce the reproduction of copepods by releasing aldehydes (Miralto et al., 1999). Although this observation could not be repeated by other studies (Irigoien et al., 2002), the effect of foraminifera and pteropods on the rain ratio should be taken into consideration, as these organisms are also important carbonate producers in the ocean (Table 1).

The total fluxes of calcium carbonate and organic carbon were measured by moored sediment traps in the western, central and eastern Arabian Sea at a ~3000 m water-depth. The calculated organic carbon/calcium carbonate carbon (POC/PIC) ratio was interpolated to the surface with the help of calcium carbonate carbon and organic car-

bon dissolution ratios determined in the water column (Hupe and Karstensen, 2000; Rixen et al., accepted, 2005). In this study data collected during the international JGOFS surveys will be used to verify the interpolated rain ratios and to investigate surface ocean processes affecting the rain and the Redfield ratio in the Arabian Sea upwelling system.

2. Study area

The Arabian Sea is strongly influenced by the Asian monsoon. This climatic feature is driven by the sea-level pressure difference between the Asian landmass and the Indian Ocean (Ramage, 1971, 1987). During the boreal winter the sea level pressure over Asia exceeds that over the Indian Ocean due to a stronger cooling of the landmass. Following the pressure gradient and deflected by the Coriolis force, the wind blows from the NE (NE monsoon) over the Arabian Sea. This situation reverses when the summer heating of the Asian landmass leads to the formation of one of the strongest atmospheric lows on Earth. This low attracts the SE trade winds, and after crossing the equator the former SE winds blow as SW winds over the Arabian Sea due to associated changes of the Coriolis force. The SW winds (SW monsoon) form a low level jet (Findlater Jet) extending almost parallel to the Arabian coast (Findlater, 1977; Rixen et al., 1996). The monsoon winds and the deserts surrounding the western and northern parts of the Arabian Sea lead to dust inputs into the Arabian Sea, which are among the highest in the world ocean (Tegen and Fung, 1994, 1995).

Biological productivity within the Arabian Sea is determined by the interplay between the euphotic zone and mixed layer depth (MLD), whose deepening is caused by winter cooling and wind mixing (Rixen et al., 2002). The interplay between the euphotic zone and the MLD regulating the availability of light and nutrients is well known from the temperate ocean. In the Arabian Sea this leads to early and late NE monsoon blooms. During the SW monsoon the Findlater Jet creates one of the most productive upwelling areas in the ocean (Antoine et al., 1996) and a hot spot for CO_2 emission along the

Arabian coast (Körtzinger et al., 1997; Goyet et al., 1998a, b; Sabine et al., 2000). Diatom blooms are common during the later phases of the NE and SW monsoon, when deep mixing and strong upwelling inject sufficient silicon from greater depths into the euphotic zone of the Arabian Sea (Haake et al., 1993b; Rixen et al., 2000).

3. Data base, methods and results

Nutrient (Morrison et al., 1998) and plankton data (Garrison et al., 2000) collected along a transect from the Arabian coast towards the southern Arabian Sea (Fig. 1) allow the study of Si/N uptake ratio of diatoms and its relation to environmental settings during the SW monsoon 1995 (14 August 1995–13 September 1995; cruise TTN50). Nutrients, total dissolved inorganic carbon (DIC), total alkalinity (TA), and CO_2 partial pressure in the atmosphere (pCO_{2air},) and surface water (pCO_{2water}) measured along the same transect approximately one month earlier (18 July 1995–13 August 1995; cruise TTN49; Goyet et al., 1998b, 1999; Millero et al., 1998) facilitate determination of Redfield and rain ratios. Finally, sediment trap experiments carried out along the transect (Nair et al., 1989; Lee et al., 1998; Honjo et al., 1999; Rixen et al., 2002) make it possible to study the impacts of surface ocean processes on the deep sea, which is the major marine carbon reservoir.

Nutrients, DIC, TA, temperature, and salinity profiles measured at the sampling sites S1–S15 during the cruises ttn49 and ttn50 were obtained from the U.S. JGOFS database. The mixed layer depth was defined as the depth at which a pronounced temperature decrease and nutrient increase occurred within profiles. Subsequently all data were averaged for the mixed layer depth (Table 2). The resulting mean mixed layer temperatures and salinities increase generally from the coastal upwelling zone towards the open ocean (Fig. 2). During both cruises slightly reduced temperatures and salinities occurred between stations S5 and S7, approximately 500 km offshore. As shown by satellite-derived SSTs charts (Fig. 2), this anomaly was probably associated with the filament that extended almost parallel to the transect, perpendicular to the

coast towards the open Arabian Sea. Despite this anomaly, the coldest and freshest water occurs at the station nearest to the coast (S1), and warm, high salinity waters characterise the most offshore sampling sites S13–S15.

The mean mixed layer nutrient concentrations decrease generally from the coastal upwelling zone towards the open ocean due to biological consumption and mixing between nutrient-enriched upwelled water and oligotrophic offshore water (Fig. 3a).

In order to distinguish between physical and biological impacts on the nutrient concentration a two-end-member mixing analysis was performed. A mixing of two water masses is indicated by a linear correlation between temperature and salinity if latent and sensible heat fluxes between the ocean and atmosphere are absent or of minor importance. In the western Arabian Sea heat fluxes (sensible and latent) reach values of approximately 100 Wm^{-2} $month^{-1}$ during the SW monsoon as indicated by satellite data (Graßl et al., 2000). Due to these ocean-atmosphere interactions temperature and salinity data are not correlated along the transect (Fig. 4). Temperature und salinity (T/S) data derived from the sampling sites S2–S14 deviate from the line that connects T/S data obtained from the sampling site S1 and S15. These deviations increase with increasing salinity until it reached a maximum and subsequently starts to decrease with further increasing salinity. The first increase seem to reflect the increasing age of the surface water and an associated enhanced heat loss from the mixed layer whereas the following decrease probably indicate a higher contribution of water from the oligotophic region. However, latent heat fluxes do not affect the relationship between salinity and nutrient concentrations as changes in the amount of water in the mixed layer increase both the salinity and the nutrient concentration. Since in addition to that salinity and nutrient concentration are unaffected by sensible heat flux, salinity instead of temperature was used to define the end-members and to calculate the mixing ratios 'a' and 'b' within the two-end-member mixing analysis at sampling sites S1–S13 ($Salinity_{S1-S13}=a_{S1-S13}$*$Salinity_{upwelled\ water}+b_{S1-S13}$ $Salinity_{oligotrophic\ water}$, whereas $a_{S1-S13}+b_{S1-S13}=1$). Station S1 was defined as the upwelling and station S13 as the oligotrophic end-member because there are hardly

any discernible variations in the salinity between stations S13, 14 and 15 (Table 2). A mixing ratio 'b' of zero indicates pure upwelled water whereas a mixing ratio 'b' of one implies that no upwelled water is present (e.g. Fig. 3a). The mixing ratios 'a' and 'b' determined for each station and the mean nutrient concentration calculated at the station S1 and S13 (see Table 2) were subsequently used to calculate a mixing line ($Phosphate_{S1-S13mixing}=a_{S1-S13}$*$Phosphate_{S1}+b_{S1-S13}$ $Phosphate_{S13}$; Fig. 3b). The mixing line represents the concentration that could be expected if mixing were the only factor controlling the nutrient concentration. Deviations of measured phosphate, inorganic nitrogen, and silicon concentrations from the mixing line can be attributed to biological consumption. In order to determine error ranges of the derived biological consumption caused by analytical methods, a relative percentage error of 0.5% and 0.012% of nutrient and salinity data (U.S. JGOFS data base documentation) was considered. Within these error ranges random errors were produced by applying the standard fortran 77 random number generator (F77-RNG). Subsequently, the mixing analysis was performed 500 times by using the produced errors. The mean ratios of inorganic nitrogen and phosphate consumptions (N/P ratios) vary between 8 and 24 (Fig. 5b) and fall within the range of N/P ratios determined in marine particulate matter and phytoplankton (~4–34; Greider and La Roche, 2002; Klausmeier et al., 2004). The resulting standard deviations of the N/P ratios are between 0.1 and 0.4.

The DIC and TA data were treated in the same way as nutrient data, but prior to calculating the biological consumption the DIC concentrations were corrected for CO_2 emission. A correction for the penetration of anthropogenic CO_2 was neglected because of the short time scale covered by the cruises. The CO_2-corrected DIC and TA consumption ($DIC_{consumption}$, $TA_{cons.}$) can be used for differentiating between the net organic carbon production ($POC_{production}$) and the precipitation of calcium carbonate ($PIC_{precipitation}$), according to the equations:

$$DIC_{consumption}=POC_{production} + PIC_{precipitation} \quad (1)$$

$$PIC_{precipitation}=(TA_{cons.} + POC_{production} * 0.15)/2 \quad (2)$$

The factor 0.15 accounts for the increase of TA during the production of organic matter, and the factor 2 due to the fact that for each mole of carbonate precipitated from the sea water TA decreases by two units (Broecker and Peng, 1982; Zeebe and Wolf-Gladrow, 2001). With two equations and two unknowns the production of organic carbon ($POC_{production}$) can be determined as follows:

$$POC_{production} = (DIC_{corrected} - TA_{cons.}/2)/1.08 \quad (3)$$

However, first the CO_2 emission was derived from ΔpCO_2 data published for each water sampling site within the U.S. JGOFS database (Table 2). The required wind-dependent gas transfer velocity 'k' was calculated using eight different formulations (Liss and Merlivat, 1986; Wanninkhof, 1992; Wanninkhof and McGillis, 1999; Nightingale et al., 2000; Feely et al., 2001). Satellite-derived wind speeds were taken from Rixen et al. (1996). The standard deviation and the resulting mean CO_2 emission at each sampling site along the transect are given in Fig. 6. In order to estimate the amount of CO_2 that escaped from the surface water, how long the water was in contact with the atmosphere must be known. It was assumed that the upwelled water is already 4 days old when it starts to advect offshore with a mean speed of 0.2–0.8 m s^{-1} (Rixen et al., 2000). The distance from the coast towards the most offshore station (S13) is ~1100 km, and the distance to the station closest to the coast (S1) is ~26 km (Table 2). Since the upwelled water within the filament seems to be younger than the surrounding water, the distance and thus the age of the surface water at each sampling site was linearly interpolated by assuming that the salinity of 36.6 represents a distance of ~1100 km, and a salinity of 35.7 represents a distance of ~26 km (see Table 2, ttn49; distance [km]=1135.1*Salinity−40451.8). The time since the water mass was in contact with the atmosphere was obtained by dividing the corrected distance by the mean advection velocity (0.6 m s^{-1}). The resulting mean CO_2 emission was subtracted from the amount of DIC held in the mixed layer and the corrected DIC concentrations were used for the two-end-member mixing analysis. Subsequently, the resulting biological DIC consumption in addition to the biological impact on the TA was used to calculate

the carbonate (PIC) and organic carbon (POC) production in the mixed layer according to the equations given above. Error ranges were determined by producing 'analytical' errors artificially by applying the F77-RNG within the range of the standard deviation given for the determination of DIC concentrations ($\pm 1.2\ 10^{-6}$ mol kg^{-1}) and TA ($\pm 3.2\ 10^{-6}$ eq. kg^{-1} Millero et al., 1998; U.S. JGOFS data base documentation). Subsequently the errors were used to re-calculate the POC and PIC production 500 times for each of the different gas transfer velocity coefficients cited above. The resulting mean C/P and rain ratios and their standard deviations are given in Fig. 5. The mean C/P uptake ratios vary between 80 and 150 and are well within the range of published C/P ratios observed in marine particulate matter and phytoplankton. The same holds true for the rain ratios which vary between ~4.2 and ~8.1 (Fig. 5c) except at station S11 where the rain ratio is 22.3 (Fig. 5c). However, due to the low carbon consumption the standard deviation at the sampling sites S10–S12 (proportion of oligotrophic water >0.7) are so high that these data have to be treated with caution within the following discussion.

In order to calculate the new production rate (Dugdale and Goering, 1967) the $POC_{production}$ (see Eq. 3) was integrated over the depth of the mixed layer and subsequently divided by the age of the upwelled water. The comparison with primary and export production rates measured at the same time and at the same stations (Buesseler et al., 1998) show that the resulting new carbon production rates are lower than the primary production rates, as expected (Fig. 7). Since new production (Eppley and Peterson, 1979) exceeds export production rates it is assumed that the biomass is growing in the mixed layer but under different environmental conditions. How the latter will effect the Redfield and rain ratios along the transect will be discussed in the following section in order to validate model assumptions and subsequently model results contributing significantly to our present understanding of climate change.

4. Discussion

Data obtained from the central Arabian Sea surface mooring (Dickey et al., 1998) show that cruise ttn49 took place at the time of monsoon-driven upwelling in the open western Arabian Sea as indicated by the shoaling of the mixed layer (Fig. 8). This corresponds with a peak of organic carbon flux and moderate carbonate/biogenic opal ratios in the western Arabian Sea, considering a time-lag of 2 weeks between surface- and deep-ocean processes. Cruise ttn50 appears to coincide with the highest organic fluxes measured during the SW monsoon period and the lowest carbonate/biogenic opal ratios. Plankton counts (Garrison et al., 2000) show that diatoms dominated the planktonic community from approximately 50 to 400 km offshore during this time (Fig. 9b). Within this diatom-dominated region, the silicon consumption exceeds the inorganic nitrogen consumption (Fig. 9a). Assuming that the contribution of diatoms to the planktonic community (=CD% see Fig. 9b) equals their contribution at the inorganic nitrogen consumption the Si/N uptake ratios of diatoms can be calculated by dividing the inorganic nitrogen consumption of diatoms by the silicon consumption ($Si_{consumption}$/[$TN_{consumption}$*(CD/100)]). The resulting Si/N uptake ratios varying between 2 and 6 (Fig. 9c) are more than twice as high as in the upwelling system of the equatorial Pacific Ocean (Dugdale and Wilkerson, 1998; Hutchins and Bruland, 1998), but close to those obtained in the Southern Ocean (Pondaven et al., 2000). However, after the silicon concentration in the surface water reaches its oligotrophic intermonsoon value of $\sim 2\,\mu mol\,kg^{-1}$, flagellates succeed diatoms in the central Arabian Sea (compare Fig. 9b and d). This observation confirms experimental data suggesting a silicon-threshold of $\sim 2\,\mu mol\,kg^{-1}$ for the dominance of diatoms within the planktonic community (Egge and Aksnes, 1992). Nevertheless, the Si/N uptake ratio of ~6 occurring after the transition towards a system dominated by flagellates does not agree with the concept of silicon-limitation. A possible explanation could be that diatom growth rates fall below diatom grazing rates (Roman et al., 2000) when silicon concentration drop below $\sim 2\,\mu mol\,kg^{-1}$. This suggests that silicon acts as a limiting nutrient for di-

atom blooms, but not for the growth of individual diatoms in the Arabian Sea. However, the lowest Si/N uptake ratios occur approximately 900 km offshore (Fig. 9c), where the iron concentration is ~25% higher than at sites closer to the coast (Fig. 9d). This indicates that as observed in enrichment experiments (Hutchins and Bruland, 1998) iron reduces the Si/N uptake ratios in the oligotrophic Arabian Sea.

During cruise ttn49, the silicon uptake and the silicon to total inorganic nitrogen uptake ratio (total Si/N ratio) were lower than during cruise ttn50 almost along the whole transect (Fig. 10a, b). Interestingly the silicon concentrations were higher during cruise ttn49 than during cruise ttn50 at 50–600 km offshore, where the difference in the silicon uptake is most pronounced (Fig. 10c). Exactly within this area, the iron concentration approaches a concentration of 2.5 nmol kg^{-1} (Fig. 10d), which was sufficient to halve the Si/N uptake ratio in an enrichment experiment (Hutchins and Bruland, 1998). Thus, the high iron concentrations seem also to hinder the silicon uptake in the Arabian Sea and this could account for the relatively low silicon export into the deep sea during cruise ttn49 (Fig. 8). To what extend the formation of thinner diatom shells or a reduced number of diatoms are responsible for the low silicon uptake and subsequently silicon export is unknown.

However, even during the cruise ttn49 slightly enhanced silicon uptake suggests that the contribution of diatoms to the plankton community is higher in the upwelling than in the oligotrophic region (Fig. 10a). This is reflected by the rain ratios which fall from 7.7 to 4.2 at the transition from the upwelling towards the oligotrophic system (Fig. 11a). The highest rain ratios occur in the oligotrophic region where inorganic nitrogen is depleted. This pattern meets the general expectation that the growth of carbonate-producing coccolithophorids is reduced by diatoms and later on by the lack of inorganic nitrogen. Rain ratios derived from sediment trap data obtained along the same transect (Rixen et al., accepted, 2005) reveal mean rain ratios of 2.4 to 3.5 during the SW monsoon 1995 (Fig. 10c). These values adjusted to a water-depth of 100 m are lower by a factor of approximately two than those obtained from the surface ocean data discussed above. The difference between the rain ratios can be explained by

the water-depth, since the mixed layer is often shallower than 100 m and the POC/PIC ratios tend to decrease within increasing water depth as the decomposition of organic matter is faster than the dissolution of carbonates in the upper water column. Moreover, the sediment trap data represent the whole SW monsoon whereas the surface ocean data reflect a shorter period of time during the SW monsoon and thus could reflect short-term extremes. However, the sediment trap and the surface ocean data reveal a decrease of the rain ratios by 30 and 45%, during the transition from the upwelling towards the oligotrophic sites (Fig. 12a). In the oligotrophic region, the high rain ratios derived from the surface ocean data are not mirrored by the sediment trap data. In contrast, the rain ratios based on sediment trap data reveal the lowest values in this region, supporting the assumption that cyanobacteria are rapidly remineralized in the upper water column and hardly sink into the deep sea (Karl et al., 1996, 1997).

Due to the preferential decomposition of more labile nitrogen containing compounds in the water column (Lee and Cronin, 1982; Wakeham et al., 1997; Lee et al., 2000) the C/N ratio obtained from sediment trap data are higher than the one derived from the surface ocean data in the oligotrophic region (Fig. 12). Vice versa C/N ratios decreasing with depth imply a preferential decomposition carbon-rich material in the upwelling area. Such carbon-enriched organic matter could be transparent exopolymers (TEP) which are produced by diatoms and foster the formation of fast-sinking marine snow (Passow et al., 1994, 2001). The formation of TEP or other carbon-enriched organic matter raises also the C/P ratios which reveal a drop from values >108 to 78 at the transition from the upwelling towards the oligotrophic system (Fig. 5a). The huge decrease of the C/P and C/N ratios is not reflected in the C/N ratios of the exported matter in the deep sea which show only a ~7% decrease at the transition from the upwelling towards the oligotrophic system (Fig. 11b). This implies that the preferential decomposition of TEP-like organic matter in the upper water column reduces the impact of diatom blooms on the Redfield ratio in the exported matter. Nevertheless even a 7% increase of the Redfield ratio associated with 30% increase of the POC/PIC ratios should have a relevant impact on concentration of the atmospheric CO_2.

5. Conclusions

It could be shown that along the transect

- diatoms increase the biologically mediated uptake of atmospheric CO_2 by enhancing the Redfield and rain ratios;
- diatom blooms seem to be terminated by the lack silicon in the euphotic zone;
- Si/N uptake ratios of diatoms vary between 2 and 6 and are getting reduced when the iron concentration in the surface water increases.

These results agree with the hypothesis that enhanced eolian iron inputs increase the availability of silicon by reducing the Si/N uptake ratio of diatoms. Furthermore our results support the assumption that diatom blooms enhance the biologically mediated uptake of atmospheric CO_2 by reducing the precipitation of carbonate and additionally increasing the Redfield ratio. On the other hand site, the Arabian Sea data indicate that enhanced iron concentrations hinder the silicon consumption and probably the development of diatom blooms. To what extend enhanced iron concentrations in the surface water attenuates an increased biologically mediated uptake of atmospheric CO_2 by lowering the increase of Redfield and rain ratios has to be investigated in future studies.

Acknowledgements. We would like to thank all the scientists, technicians, and officers and their crews of the numerous research vessels as well as the national funding agencies who made the Joint Global Ocean Flux Study in the Arabian Sea possible. Particularly, we would like to appreciate the work of S. Honjo, S. Manganini, T. Dickey, K. Buesseler, C. I. Measures, S. Vink, J. M. Morrison, D. L. Garrison and L. Codispoti, which in particular contributed to our study. We would like to thank also C. Lee and S. W. A. Naqvi for helpful discussions. Furthermore, we are grateful to the Federal German Ministry for Education, Science, Research and Technology (BMBF, Bonn) and the German Research Council (DFG, Bonn), the Council of Scientific and Industrial Research (CSIR, New Delhi), and the Department of Ocean Development (DOD, New Delhi) for financial support of the Bilateral Indo/German Program on Biogeochemical Fluxes in

the northern Indian Ocean. P. Wessels and W. H. F. Smith are acknowledged for providing the generic mapping tools (GMT), as well as B. Aksen for secretarial assistance.

References

Anderson, L. A. and Sarmiento, J. L.: Redfield ratios of remineralization determined by nutrient data analysis, Global Biog., 8 (1), 65–80, 1994.

Antoine, D., André, J.-M., and Morel, A.: Oceanic primary production – 2. Estimation at global scale from satellite (coastal zone color scanner) chlorophyll, Global Biog., 10 (1), 57–69, 1996.

Archer, D., Winguth, A. M. E., Lea, D., and Mahowald, N.: What caused the glacial/interglacial atmospheric pCO_2 cycles?, Rev. Geophys., 38 (2), 159–189, 2000.

Berger, W. H. and Keir, R. S.: Glacial-Holocene Changes in Atmospheric CO_2 and the Deep-Sea Record, in: Climate Processes and Climates Sensitivity, edited by: Hansen, J. E. and Takahashi, T., 337–351, Am. Geophys. Union, Washington, 1984.

Broecker, W. S. and Peng, T.-H.: Tracers in the sea, Lamont-Doherty Geological Observatory, Columbia University, Palisades, New York, 690, 1982.

Buesseler, K., Ball, L., Andrews, J., Benitez-Nelson, C., Belastock, R., Chai, F., and Chao, Y.: Upper ocean export of particulate organic carbon in the Arabian Sea derived from thorium-234, Deep-Sea II, 45 (10–11), 2461–2487, 1998.

Burkhardt, S., Zondervan, I., and Riebesell, U.: Effect of CO_2 concentration on C: N: P ratio in marine phytoplankton: A species comparison, Limn. Ocean., 44 (3), 683–690, 1999.

Conley, D. J.: Terrestrial ecosystems and the biogeochemical silica cycle, Global Biog., 16 (4), 1–8, 2002.

Dickey, T., Marra, J., Sigurdson, D. E., Weller, R. A., Kinkade, C. S., Zedler, S. E., Wiggert, J. D., and Langdon, C.: Seasonal variability of bio-optical and physical properties in the Arabian Sea: October 1994–October 1995, Deep-Sea II, 45 (10–11), 2001–2025, 1998.

Dugdale, R. C. and Goering, J. J.: Uptake of new and regenerated forms of nitrogen in primary productivity, Limn. Ocean., 12, 196–206, 1967.

Dugdale, R. C. and Wilkerson, F. P.: Silicate regulation of new production in the equatorial Pacific upwelling, Nature, 391, 270–273, 1998.

Egge, J. K. and Aksnes, D. L.: Silicate as regulating nutrient in phytoplankton competition, Mar. Ecol.-PR., 83, 281–289, 1992.
Eppley, R. W. and Peterson, B. J.: Particulate organic matter flux and planktonic new production in the deep ocean, Nature, 282, 677–680, 1979.
Falkowski, P., Scholes, R. J., Boyle, E., Canadell, J., Canfield, D., Elser, J., Gruber, N., Hibbard, K., Högberg, P., Linder, S., Mackenzie, F. T., Moore III, B., Pedersen, T., Rosenthal, Y., Seitzinger, S., Smetacek, V., and Steffen, W.: The Global Carbon Cycle: A Test of Our Knowledge of Earth as a System, Science, 290, 291–296, 2000.
Feely, R. A., Sabine, C. L., Takahashi, T., and Wanninkhof, R.: Uptake and storage of carbon dioxide in the ocean: The global survey, Oceanography, 14 (4), 18–32, 2001.
Findlater, J.: Observational Aspects of the Low-level Cross-equatorial Jet Stream of the Western Indian Ocean, Pageoph., 115, 1251–1262, 1977.
Froelich, P. N., Blanc, V., Mortlock, R. A., and Chillrud, S. N.: River fluxes of dissolved silica to the ocean were higher during glacials: Ge/Si in diatoms, rivers, and oceans, Paleo Oceanog., 7 (6), 739–767, 1992.
Garrison, D. L., Gowing, M. M., Hughes, M. P., Campbell, L., Caron, D. A., Dennett, M. R., Shalapyonok, A., Olson, R. J., Landry, M. R., and Brown, S. L.: Microbial food web structure in the Arabian Sea: a US JGOFS study, Deep-Sea II, 47 (7–8), 1387–1422, 2000.
Goldman, J. C., McCarthy, J. J., and Peavey, D. G.: Growth rate influence on the chemical composition of phytoplankton in oceanic waters, Nature, 279, 210–214, 1979.
Goyet, C., Millero, F. J., O'Sullivan, D. W., Eischeid, G., McCue, S. J., and Bellerby, R. G. J.: Temporal variations of pCO_2 in surface seawater of the Arabian Sea in 1995, Deep-Sea I, 45 (4–5), 609–623, 1998a.
Goyet, C., Metzl, N., Millero, F., Eischeid, G., O'Sullivan, D., and Poisson, A.: Temporal variation of the sea surface CO2/carbonate properties in the Arabian Sea, Mar. Chem., 63 (1–2), 69–79, 1998b.
Goyet, C., Coatanoan, C., Eischeid, G., Amaoka, T., Okuda, K., Healy, R., and Tsunogai, S.: Spatial variation of total CO_2 and total alkalinity in the northern Indian Ocean: A novel approach for the quantification of anthropogenic CO_2 in seawater, J. Mar. Re., 57, 135–163, 1999.
Graßl, H., Jost, V., Kumar, R., Schulz, J., Bauer, P., and Schlüssel, P.: The Hamburg Ocean-Atmosphere Parameters and Fluxes from Satellite Data (HOAPS): A climatological atlas od satellite-derived air-sea-interaction parameters over the ocean, Max-Planck-Institute für Me-

teorologie, Hamburg, 128, 2000.
Greider, R. J. and La Roche, J.: Redfield revisited: variability of C:N:P in marine microalgae and its biochemical basis, European Journal of Phycology, 37, 1–17, 2002.
Haake, B., Rixen, T., and Ittekkot, V.: Variability of moonsonal upwelling signals in the deep western Arabian Sea, SCOPE/UNEP Sonderband, 76, 85–96, 1993a.
Haake, B., Ittekkot, V., Rixen, T., Ramaswamy, V., Nair, R. R., and Curry, W. B.: Seasonality and interannual variability of particle fluxes to the deep Arabian Sea, Deep-Sea I, 40 (7), 1323–1344, 1993b.
Harrison, K. G.: Role of increased marine silica input on paleo-pCO_2 levels, Paleo Oceanog, 15 (3), 292–298, 2000.
Hedges, J. I., Baldock, J. A., Gelinas, Y., lee, C., Peterson, M. L., and Wakeham, S. G.: The biochemical and elemental composition of marine plankton: A NMR perspective, Mar. Chem., 78, 47–63, 2002.
Heinze, C., Maier-Reimer, E., and Winn, K.: Glacial pCO_2 Reduction by the World Ocean: Experiments with the Hamburg Carbon Cycle Model, Paleo Oceanog, 6 (4), 395–430, 1991.
Honjo, S., Dymond, J., Prell, W., and Ittekkot, V.: Monsoon-controlled export fluxes to the interior of the Arabian Sea, Deep-Sea II, 46 (8–9), 1859–1902, 1999.
Hupe, A. and Karstensen, J.: Redfield stoichiometry in Arabian Sea subsurface waters, Global Biog., 14 (1), 357–372, 2000.
Hutchins, D. A. and Bruland, K. W.: Iron-limited diatom growth and Si:N uptake ratios in a costal upwelling regime, Nature, 393, 561–564, 1998.
Irigoien, X., Harris, R. P., Verheye, H. M., Joly, P., Runge, J., Starr, M., Pond, D., Campbell, R., Shreeve, R., Ward, P., Smith, A. N., Dam, H. G., Peterson, W., Tirelli, V., Koski, M., Smith, T., Harbour, D., and Davidson, R.: Copepod hatching success in marine ecosystems with high diatom concentrations, Nature, 419, 387–389, 2002.
Karl, D., Letelier, R., Tupas, L., Dore, J., Christian, J., and Hebel, D.: The role of nitrogen fixation in biogeochemical cycling in the suptropical North Pacific Ocean, Nature, 388, 533–538, 1997.
Karl, D. M., Christian, J. R., Dore, J. E., Hebel, D. V., Letelier, R. M., Tupas, L. M., and Winn, C. D.: Seasonal and interannual variability in primary production and particle flux at Station ALOHA, Deep-Sea II, 43 (2–3), 539–568, 1996.
Klausmeier, C. A., Lichtman, E., Daufresne, T., and Levin, S. A.: Optimal nitrogen-to-phosphorus stoichiometry of phytoplankton, Nature, 429, 171–174, 2004.

Körtzinger, A., Duinker, J. C., and Mintrop, L.: Strong CO_2 emissions from the Arabian Sea during south-west monsoon, Geophys. Res. Lett., 24 (14), 1763–1766, 1997.
Lee, C. and Cronin, C.: The vertical flux of particulate organic nitrogen in the sea: decomposition of amino acids in the Peru upwelling area and the equatorial Atlantic, J. Mar. Re., 40 (1), 227–251, 1982.
Lee, C., Murray, D. W., Barber, R. T., Buesseler, K. O., Dymond, J., Hedges, J. I., Honjo, S., Manganini, S. J., and Marra, J.: Particulate organic carbon fluxes: compilation of results from the 1995 US JGOFS Arabian Sea Process Study, Deep-Sea II, 45 (10–11), 2489–2501, 1998.
Lee, C., Wakeham, S. G., and Hedges, J. I.: Composition and flux of particulate amino acids and chloropigments in equatorial Pacific seawater and sediments, Deep-Sea I, 47 (8), 1535–1568, 2000.
Liss, P. S. and Merlivat, L.: Air-sea gas exchange rates: Introduction and synthesis, in: The Role of Air-Sea Exchange in Geochemical Cycling, edited by: Buat-Mernard, P., Reidel, Boston, 113–129, 1986.
Maier-Reimer, E.: Dynamic vs. apparent Redfield ratio in the oceans: A case for 3D-models, J. Mar. Sys., 9, 113–120, 1996.
Maier-Reimer, E., Mikolajewicz, U., and Winguth, A.: Future ocean uptake of CO_2: interaction between ocean circulation and biology, Clim. Dynam., 12, 711–721, 1996.
Matsumoto, K. and Sarmiento, J. L.: Silicic acid leakage from the Southern Ocean: A possible explanation for glacial atmospheric pCO_2, Global Biog., 16 (3), 5-1–5-23, 2002.
Millero, F. J., Degler, E. A., O'Sullivan, D. W., Goyet, C., and Eischeid, G.: The carbon dioxide system in the Arabian Sea, Deep-Sea II, 45 (10–11), 2225–2252, 1998.
Milliman, J. D. and Droxler, A. W.: Neritic and pelagic carbonate sedimentation in the marine environment: ignorant is not bliss, Geologische Rundschau, 85, 496–504, 1996.
Miralto, A., Barone, G., Romano, G., Poulet, S. A., Ianora, A., Russo, G. L., Buttino, I., Mazzarella, G., Laabir, M., Cabrini, M., and Giacobbe, M. G.: The insidious effect of diatoms on copepod reproduction, Nature, 402, 173–176, 1999.
Morrison, J. M., Codispoti, L. A., Gaurin, S., Jones, B., Manghanani, V., and Zheng, Z.: Seasonal variation of hydrographic and nutrient fields during the US JGOFS Arabian Sea Process Study, Deep-Sea II, 45 (10–11), 2053–2101, 1998.
Nair, R. R., Ittekkot, V., Manganini, S. J., Ramaswamy, V., Haake, B., Degens, E. T., Desai, B. N., and Honjo, S.: Increased particle flux to the deep ocean related to monsoons, Nature,

338 (6218), 749–751, 1989.
Nightingale, P. D., Malin, G., Law, C. S., Watson, A. J., Liss, P. S., Liddicoat, M. I., Boutin, J., and Upstill-Goddard, R. C.: In situ evaluation of air-sea gas exchange parameterizations using novel conservative and volatile tracers, Global Biog., 14, 373–387, 2000.
Passow, U., Alldredge, A. L., and Logan, B. E.: The role of particulate carbohydrate exudates in the flocculation of diatom blooms, Deep-Sea I, 41 (2), 335–357, 1994.
Passow, U., Shipe, R. F., Murray, A., Pak, D. K., Brzezinski, M. A., and Alldredge, A. L.: The origin of transparent exopolymer particles (TEP) and their role in the sedimentation of particulate matter, Cont. Shelf, 21 (4), 327–346, 2001.
Pondaven, P., Ruiz-Pino, D., Fravalo, C., Treguer, P., and Jeandel, C.: Interannual variability of Si and N cycles at the time-series station KERFIX between 1990 and 1995 – a 1-D modelling study, Deep-Sea I, 47 (2), 223–257, 2000.
Ramage, C. S.: Monsoon Meteorology, Academic Press, New York, London, 1971.
Ramage, C. S.: Monsoon Climates, in: The Encyclopedia of Climatology, edited by: Oliver, J. E. and Fairbridge, R. W., Van Nostrand Reinhold Company, New York, 1987.
Redfield, A. C., Ketchum, B. H., and Richards, F. A.: The Influence of organisms on the composition of sea-water, in: The sea, edited by: Hitt, M. N., Wiley & Sons, New York, 26–77, 1963.
Ridgwell, A. J., Watson, A. J., and Archer, D.: Modeling the response of the oceanic Si inventory to perturbation, and consequences for atmospheric CO_2, Global Biog., 16 (4), 19-1–19-15, 2002.
Rixen, T., Haake, B., Ittekkot, V., Guptha, M. V. S., Nair, R. R., and Schlüssel, P.: Coupling between SW monsoon-related surface and deep ocean processes as discerned from continous particle flux meausurements and correlated satellite data, J. Geophys. Res.-O, 101 (C12), 28 569–28 582, 1996.
Rixen, T., Haake, B., and Ittekkot, V.: Sedimentation in the western Arabian Sea: the role of coastal and open-ocean upwelling, Deep-Sea II, 47, 2155–2178, 2000.
Rixen, T., Guptha, M. V. S., and Ittekkot, V.: Sedimentation, in: Report of the Indian Ocean Synthesis Group on the Arabian Sea Process Study, edited by: Watts, L., Burkill, P. H., and Smith, S., JGOFS International Project Office, Bergen, 65–73, 2002.
Rixen, T., Guptha, M. V. S., and Ittekkot, V.: Deep ocean fluxes and their link to surface ocean processes and the biological pump, Progress in Oceanography, accepted, 2005.
Roman, M., Smith, S., Wishner, K., Zhang, X., and Gowing, M.: Mesozooplankton production

and grazing in the Arabian Sea, Deep-Sea II, 47 (7–8), 1423–1450, 2000.
Sabine, C. L., Wanninkhof, R., Key, R. M., Goyet, C., and Millero, F. J.: Seasonal CO2 fluxes in the tropical and subtropical Indian Ocean, Mar. Chem., 72 (1), 33–53, 2000.
Sarmiento, J. L., Dunne, J., Gnanadesikan, A., Key, R. M., Matsumoto, K., and Slater, R.: A new estimate of the CaCO3 to organic carbon export ratio, Global Biog., 16 (4), 54-1–54-12, 2002.
Schiebel, R.: Planktic foraminiferal sedimentation and the marine calcite budget, Global Biog., 16 (4), 13-1–13-21, 2002.
Tegen, I. and Fung, I.: Modeling of mineral dust in the atmosphere, J. Geophys. Res.-O, 99 (D11), 22 897–22 914, 1994.
Tegen, I. and Fung, I.: Contribution to the atmospheric mineral aerosol load from land surface modification, J. Geophys. Res.-O, 100 (D9), 18 707–18 726, 1995.
Tyrrell, T.: The relative influences of nitrogen and phosphorus on oceanic primary production, Nature, 400, 525–531, 1999.
Volk, T. and Hoffert, M. I.: The carbon cycle and atmospheric CO_2, natural variation archean to present, edited by: Sundquits, E. T. and Broecker, W. S., AGU, Washington, 99–110, 1985.
Wakeham, S. G., Lee, C., Hedges, J. I., Hernes, P. J., and Peterson, M. L.: Molecular indicators of diagenetic status in marine organic matter, Geochim. Cos. A, 61 (24), 5363–5369, 1997.
Wanninkhof, R.: Relationship between gas exchange and wind speed over the ocean, J. Geophys. Res.-O, 97, 7373–7381, 1992.
Wanninkhof, R. and McGillis, W. M.: A cubic relationship between gas transfer and wind speed, Geophys. Res. Lett., 26, 1889–1983, 1999.
Zeebe, R. E. and Wolf-Gladrow, D.: CO_2 In Seawater: Equilibrium, Kinetics, Isotopes, Elsevier Science B. V., Amsterdam, 346, 2001.

Table 1. Contribution of carbonate-producing organism to the pelagic marine carbonate production.

	%	10^{15} g C	References
Total carbonate production	100	0.60–0.86	Milliman and Droxler (1996)
Foraminifera	23–56	0.14–0.48	Schiebel (2002)
Pteropods	∼10	0.06–0.09	Schiebel (2002)*
Coccolithophorids	4–38	0.02–0.33	Schiebel (2002)*

* and references therein.

Table 2. Station number, position, distance between the station and the coast, mixed layer depth, mean mixed layer temperature, salinity, phosphate, total inorganic nitrogen, silicon and total inorganic carbon concentration, mean total alkalinity and partial pressure difference between the atmosphere and the ocean. Missing data are indicated by −99.00. The position was obtained by averaging the position of all available hydrographic casts at one sampling sites.

St.	Lon.	Lat.	Distance	MLD	Temp.	Sal.	PO_4	TN	Si	DIC	TA	ΔpCO_2
	(° E)	(° N)	(km)	(m)	(C)	(psu)	———	(μmol/kg)	———		μeq./kg	μatm
						Cruise ttn49						
S1	57.32	18.52	25.73	10.00	20.84	35.66	1.55	17.40	9.23	2146.50	2338.60	−299.09
S2	58.03	18.16	93.01	18.00	22.98	35.71	1.32	15.40	7.64	2111.43	2329.18	−222.65
S3	58.86	17.67	193.58	53.00	25.99	36.00	0.69	5.58	3.13	2046.65	2349.28	−99.37
S4	59.87	17.17	313.98	42.00	26.65	36.10	0.53	4.12	2.73	2044.78	2348.66	−83.25
S5	60.51	16.79	392.79	48.00	25.90	36.02	0.60	4.81	2.51	2042.92	2348.80	−89.41
S6	61.25	16.43	482.12	40.00	24.55	35.82	1.13	12.16	5.59	2091.47	2340.20	−159.56
S7	62.00	16.03	573.55	34.00	25.74	36.05	0.79	7.25	3.55	2056.73	2350.63	−116.40
S8	62.81	15.64	669.95	75.00	26.89	36.37	−99.00	1.52	1.80	2030.58	2369.00	−57.44
S9	63.51	15.23	757.38	82.00	26.66	36.29	0.44	2.01	1.25	2035.04	2362.73	−54.62
S10	64.25	14.82	849.37	83.00	26.73	36.32	0.39	0.96	1.16	2028.16	2366.69	−39.80
S11	65.00	14.44	940.11	75.00	27.28	36.47	0.32	0.51	0.99	2024.41	2375.23	−27.76
S12	65.00	13.24	1010.75	84.00	27.19	36.43	0.27	0.04	0.54	2020.13	2373.47	−27.38
S13	65.01	12.05	1092.72	108.00	27.71	36.60	0.24	0.17	0.69	2018.74	2382.50	−19.72
S14	65.00	10.81	1186.65	104.00	27.72	36.57	0.27	0.29	1.10	2020.96	2381.27	−23.93
S15	64.91	9.97	1247.93	95.00	27.88	36.58	0.25	0.40	1.19	2017.80	2381.40	−27.45
						Cruise ttn50						
S1	57.30	18.50	23.26	14.00	20.95	35.66	1.66	19.42	11.18	−99.00	−99.00	−99.00
S2	58.04	18.09	96.34	10.00	23.93	35.69	1.32	15.09	5.71	−99.00	−99.00	−99.00
S3	58.85	17.67	192.68	20.00	23.82	35.74	1.07	11.50	1.99	−99.00	−99.00	−99.00
S4	59.77	17.18	303.75	25.00	24.89	35.79	0.96	9.62	1.51	−99.00	−99.00	−99.00
S5	60.50	16.80	392.48	52.00	25.64	35.84	0.85	8.38	1.12	−99.00	−99.00	−99.00
S6	61.25	16.43	481.32	52.00	26.65	36.11	0.53	3.15	0.97	−99.00	−99.00	−99.00
S7	61.98	16.01	573.00	50.00	26.52	36.04	0.59	3.84	1.49	−99.00	−99.00	−99.00
S8	62.77	15.64	666.57	48.00	26.10	35.95	0.76	6.52	1.70	−99.00	−99.00	−99.00
S9	63.50	15.25	756.05	74.00	26.54	36.07	0.57	3.84	2.42	−99.00	−99.00	−99.00
S11	65.00	14.44	940.20	75.00	26.93	36.23	0.41	1.22	0.73	−99.00	−99.00	−99.00
S13	65.00	12.05	1091.55	102.00	27.42	36.51	0.34	0.31	0.59	−99.00	−99.00	−99.00
S14	65.00	10.80	1186.62	100.00	27.64	36.51	0.32	0.09	0.42	−99.00	−99.00	−99.00
S15	64.90	9.97	1247.66	84.00	27.85	36.57	0.30	0.13	0.27	−99.00	−99.00	−99.00

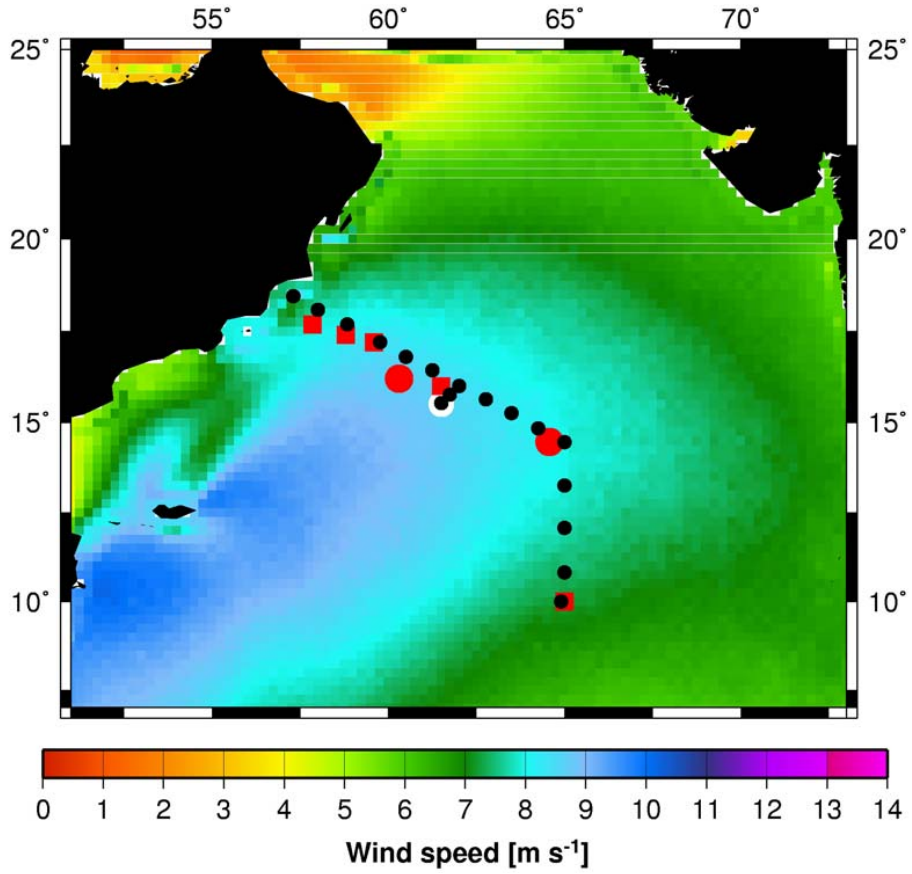

Fig. 1. Mean SW monsoon wind speeds over the Arabian Sea during the SW monsoon (data are from Rixen et al., 1996). Red squares indicate the U.S. JGOFS (Honjo et al., 1999) and the red circles the Indo/German sediment trap sites in the western and central Arabian Sea (Rixen et al., 2003). The white circle indicate the central Arabian Sea surface mooring location (Dickey et al., 1998), and the black circles show the U.S. JOGFS water sampling sites (Morrison et al., 1998).

BGD
2, 103–136, 2005

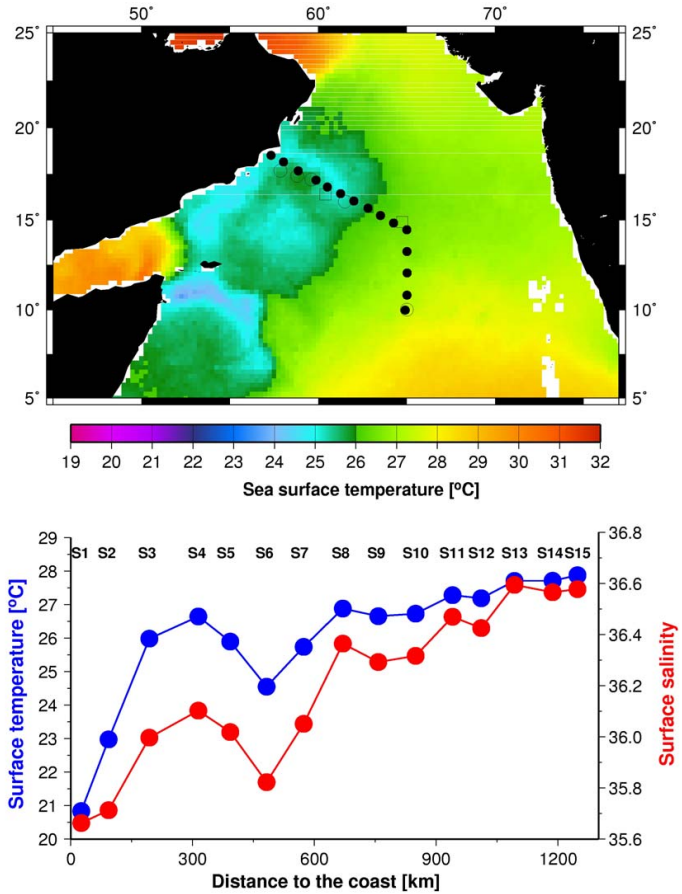

Fig. 2. Upper panel: Mean SW monsoon sea surface temperatures (data: see Rixen et al., 1996) during the cruise ttn49. Lower panel: Surface temperatures and salinity averaged for the depth of the mixed layer (data are from the U.S. JGOFS database: http://usjgofs.whoi.edu/jg/dir/jgofs/arabian/) at each sampling site (S1 to S15).

BGD
2, 103–136, 2005

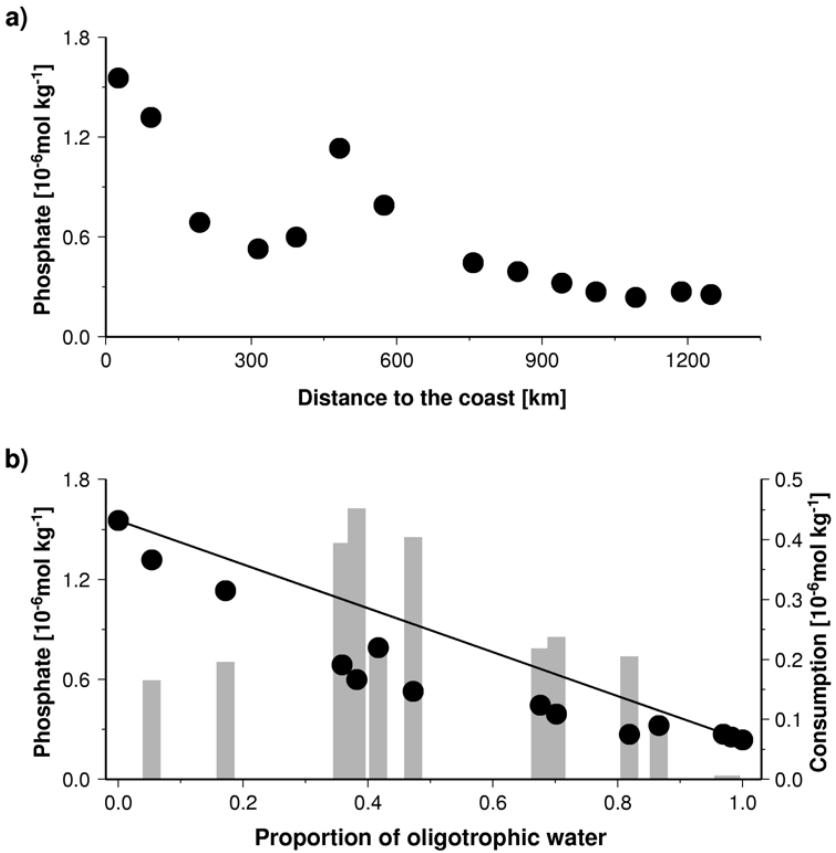

Fig. 3. (a) Phosphate concentration measured during cruise ttn49 and averaged for the depth of the mixed layer versus the distance to the coast (data are from the U.S. JGOFS database). **(b)** Mean phosphate concentration (black circles) and the mixing line (black line) versus the proportion of oligotrophic water. Bars reveal the difference between the mean phosphate concentration and the mixing line, which is regarded as biological consumption.

BGD
2, 103–136, 2005

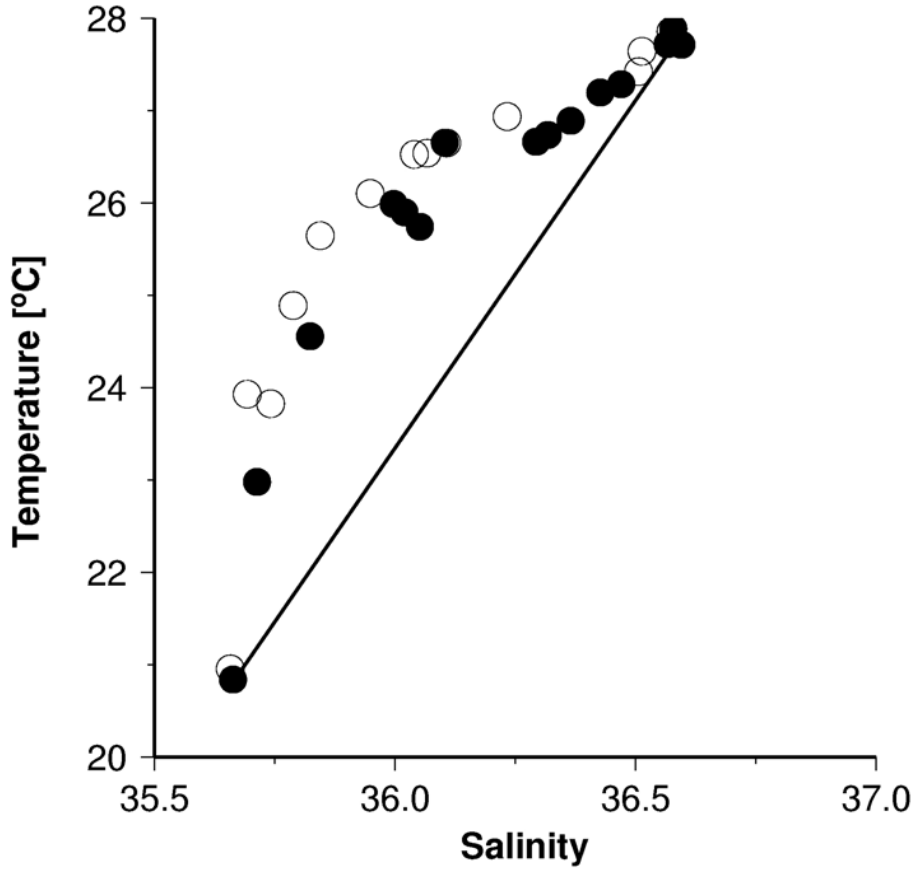

Fig. 4. Salinity versus temperature. Salinities and temperatures were measured during cruise ttn49 (open circles) and ttn50 (black circles) and averaged for the depth of the mixed layer (data are from the U.S. JGOFS database). The black line connects the data collected at the sites S1 and S13.

BGD
2, 103–136, 2005

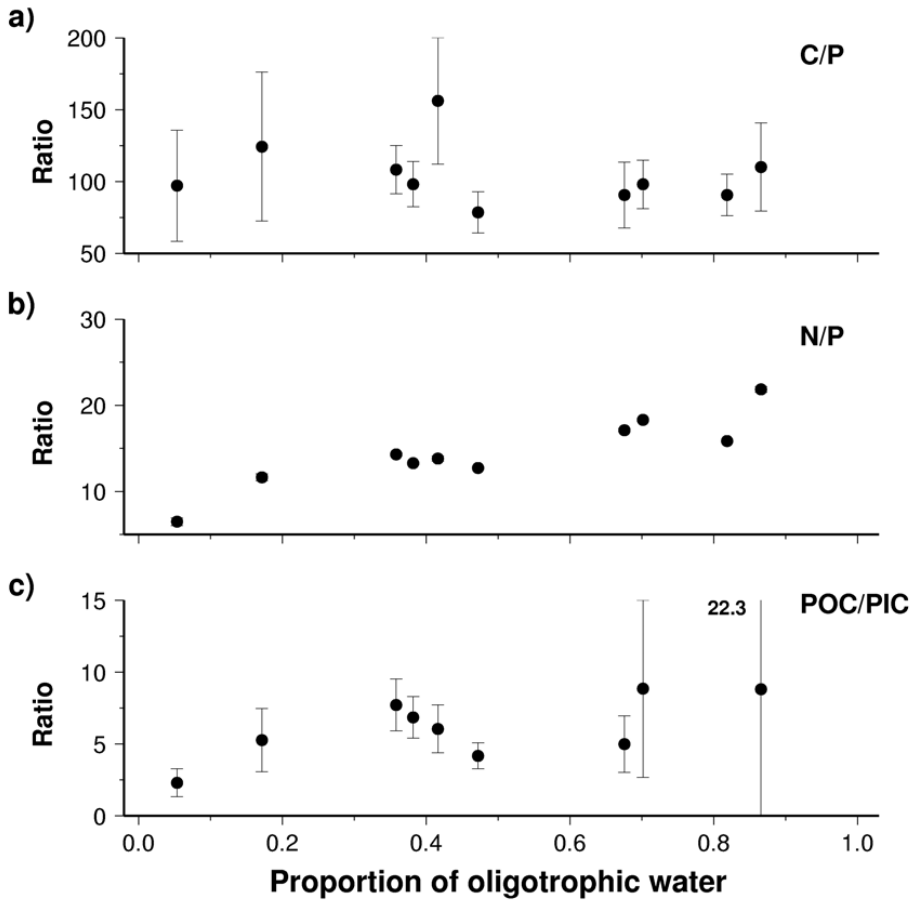

Fig. 5. (a) C/P, **(b)** N/P and **(c)** rain (POC/PIC) ratios versus the proportion of oligotrophic water. Error bars are calculated as described in the text. The number in panel (c) indicates the rain ratio at the sampling site S11 which is not plotted as it is out of scale.

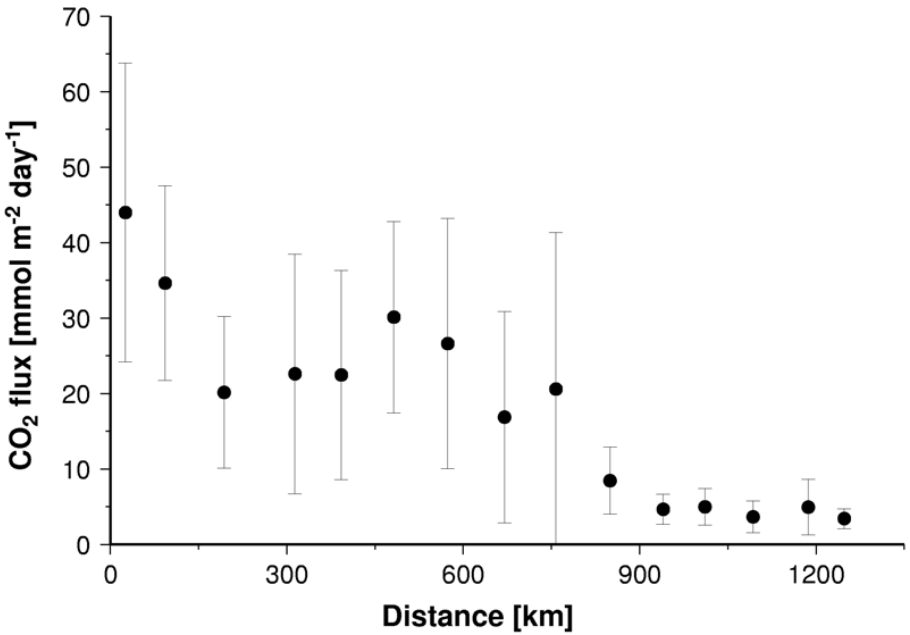

Fig. 6. Mean CO_2 emission derived from ΔpCO_2 data obtained from the U.S. JGOFS data, satellite-derived and instu wind speeds and the gas transfer velocity 'k' which was calculated after (Liss and Merlivat, 1986; Wanninkhof, 1992; Wanninkhof and McGillis, 1999; Nightingale et al., 2000) versus the distance to the coast. Error bars indicate the standard variation of results derived from the different wind speed data sets and the different methods to calculate 'k'.

BGD
2, 103–136, 2005

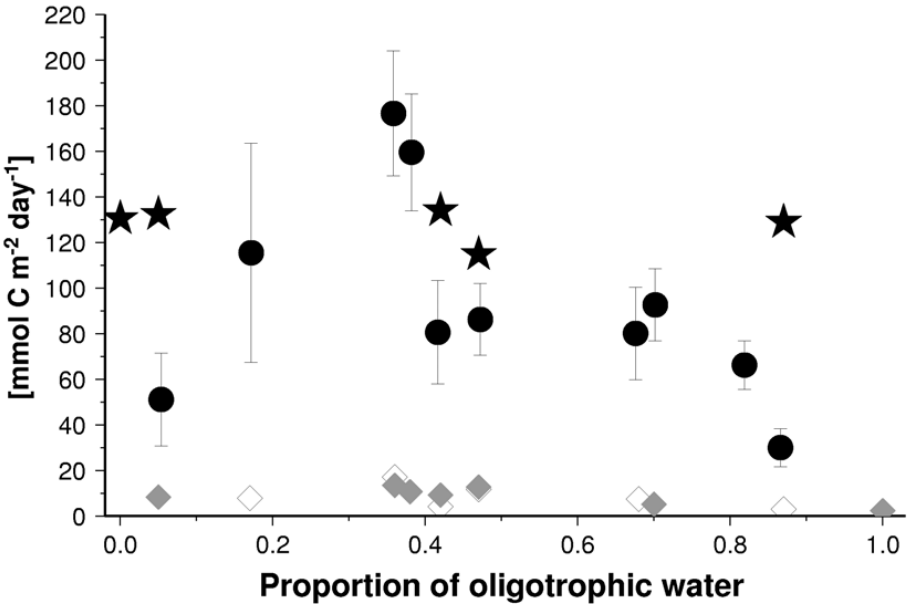

Fig. 7. Primary production rates (stars), export production rates derived from ^{234}Th measurements (open diamonds; Buesseler et al., 1998), and sediment trap data (grey diamonds; Rixen et al., 2003). Organic carbon production calculated from the DIC and TA uptake is indicated by black circles.

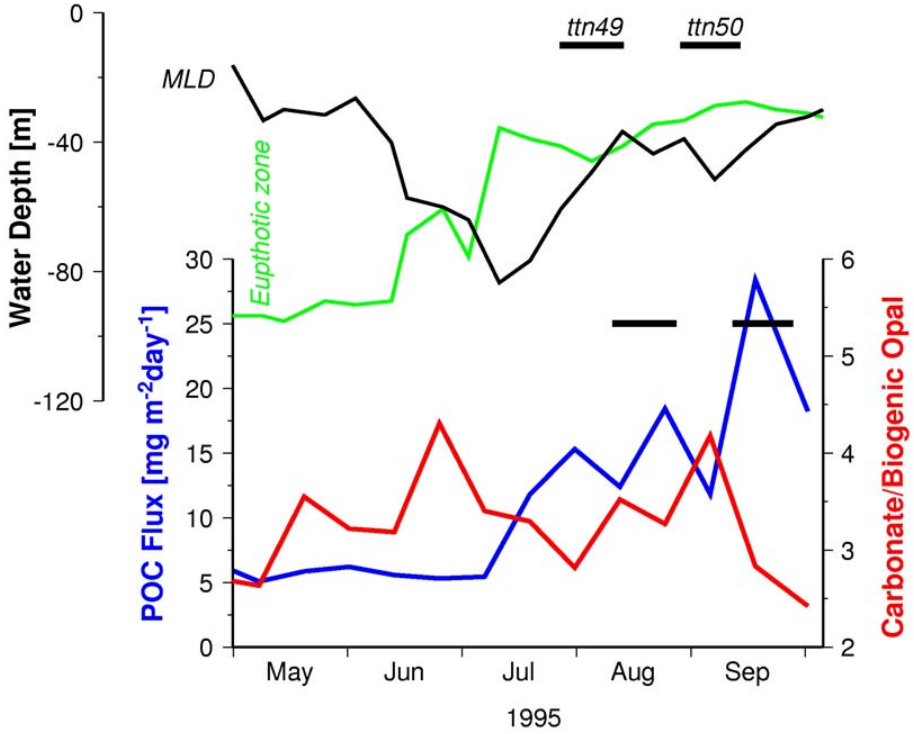

Fig. 8. Depth of the mixed layer (MLD black line) and of the euphotic zone (1% light level; green line) determined at the ONR mooring site. Data was redrawn from Dickey et al. (1998). The MLD represents the water-depth at which the temperature is 1°C lower than at the surface. The organic carbon fluxes measured at 3000 m water-depth at the western Arabian Sea trap site are indicated by the blue line, and the carbonate/biogenic opal ratios measured by the same trap are shown in red. The horizontal black lines show the time during which the cruises ttn49 and 50 have were performed and the measured surface data could be reflected in the deep ocean fluxes adding a delay of about 14 days.

BGD
2, 103–136, 2005

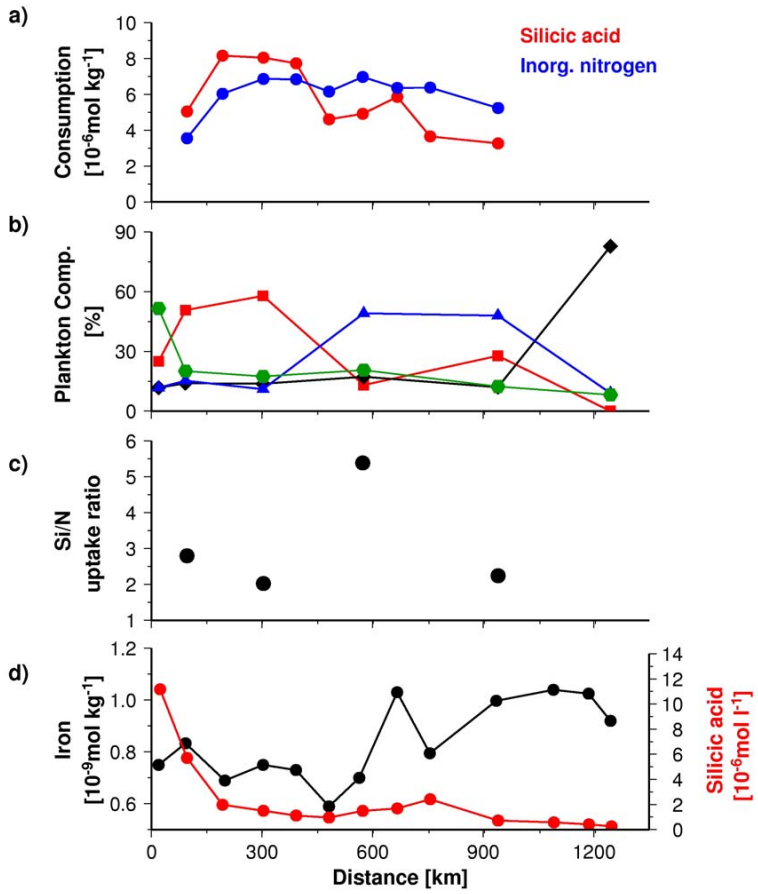

Fig. 9. **(a)** Silicon and inorganic nitrogen-consumption, **(b)** contribution of nanoplankton (green), diatoms (red), flagellates (blue) and cyanobacteria (black) to the biomass of photoautotrophic plankton, **(c)** Si/N uptake ratio and **(d)** iron and silicon concentrations (d) versus the distance to the coast during the cruise ttn50.

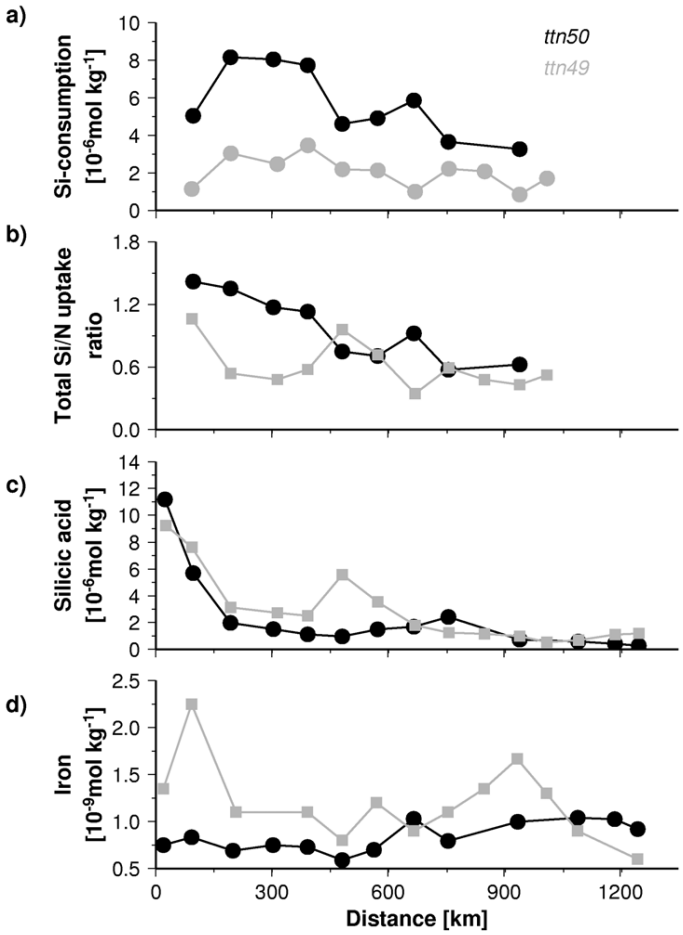

Fig. 10. (a) Silicon consumption, **(b)** total Si/N uptake ratios, **(c)** silicon and **(d)** iron concentration versus the distance to the coast during the cruises ttn49 and 50.

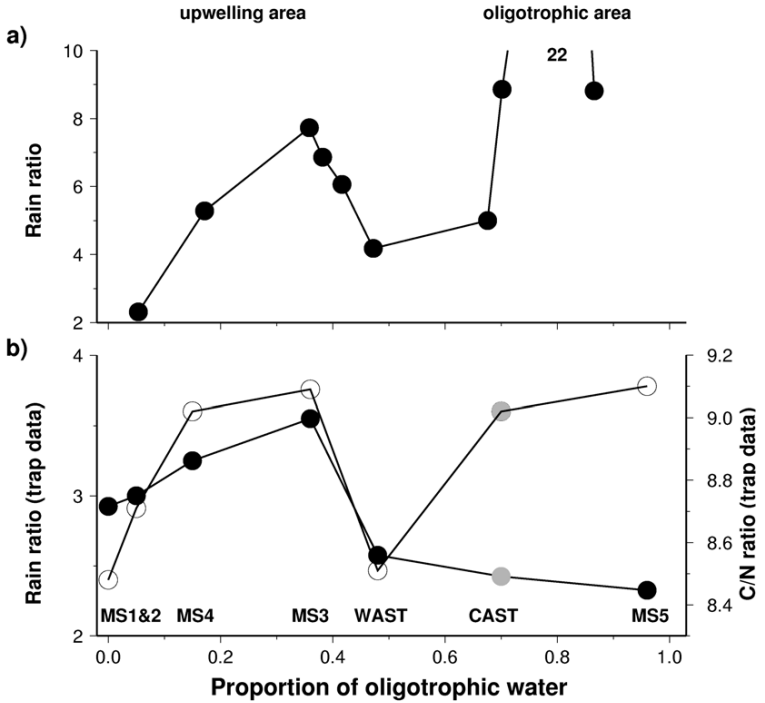

Fig. 11. (a) Rain ratios derived from the surface ocean data versus the proportion of oligotrophic water (same data as shown in Fig. 5). **(b)** POC/PIC (rain, black circles) and C/N ratios (open circles) derived from sediment traps versus the proportion of oligotrophic water data. The sediment trap data reveal the mean SW monsoon values, and their proportion of oligotrophic water was determined by adjoining to them the closest water-sampling site during the cruise ttn49. Since lateral advection has to be considered additionally, not the closest station was used but its neighbour station to the west (coast). The grey circles indicate POC/PIC and C/N ratio obtained from our central Arabian Sea station measured during the SW monsoons 1986 to 1997, but not during the SW monsoon 1995, due to an instrumental error.

BGD
2, 103–136, 2005

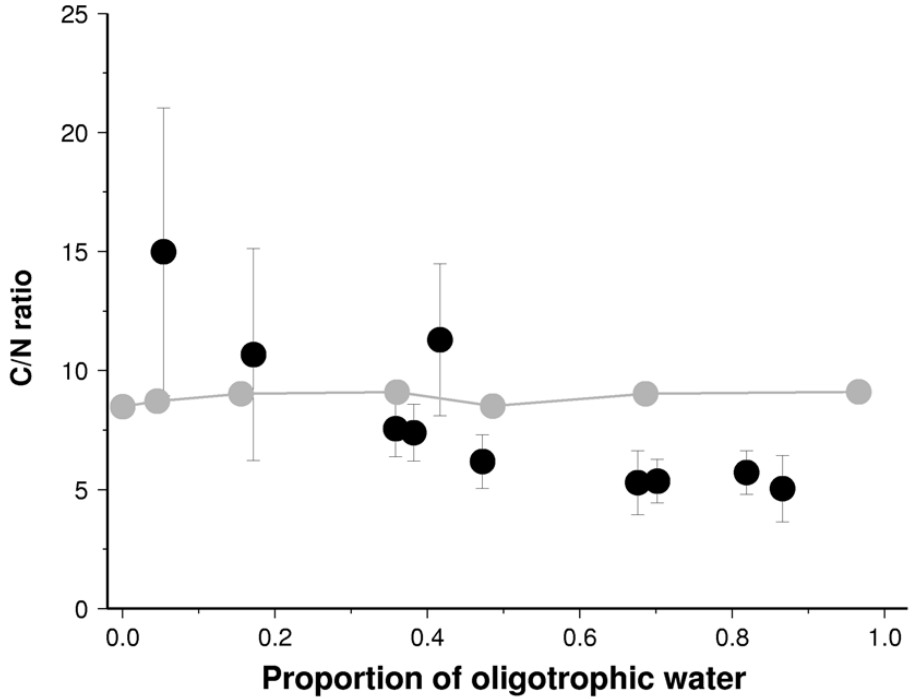

Fig. 12. C/N ratios derived from the surface ocean data (black circles) and sediments traps (grey circles) versus the proportion of oligotrophic water.

BGD

2, 103–136, 2005